nature communications

Article

https://doi.org/10.1038/s41467-024-52116-9

Water-catalyzed iron-molybdenum carbyne formation in bimetallic acetylene transformation

Received: 12 March 2024

Accepted: 26 August 2024

Published online: 04 September 2024

Check for updates

Xiaofang Zhai[1], Minghui Xue[2], Qiuting Zhao[1], Qiucui Zheng[1], Datong Song[3] ✉, Chen-Ho Tung[2] & Wenguang Wang[1] ✉

Transition metal carbyne complexes are of fundamental importance in carbon-carbon bond formation, alkyne metathesis, and alkyne coupling reactions. Most reported iron carbyne complexes are stabilized by incorporating heteroatoms. Here we show the synthesis of bioinspired FeMo heterobimetallic carbyne complexes by the conversion of C_2H_2 through a diverse series of intermediates. Key reactions discovered include the reduction of a μ-η^2:η^2-C_2H_2 ligand with a hydride to produce a vinyl ligand (μ-η^1:η^2-$CH=CH_2$), tautomerization of the vinyl ligand to a carbyne (μ-CCH_3), and protonation of either the vinyl or the carbyne compound to form a hydrido carbyne heterobimetallic complex. Mechanistic studies unveil the pivotal role of H_2O as a proton shuttle, facilitating the proton transfer that converts the vinyl group to a bridging carbyne.

Since the pioneering work of Fischer, Schrock, and et al.[1,2], transition metal alkylidyne complexes, commonly known as carbyne complexes, have found significant applications in synthetic chemistry and material science[3–9]. The exploration of abundant-metal catalysis has spurred considerable interest in synthetic iron complexes with metal-carbon bonds[10,11]. Previous studies have emphasized the importance of stabilizing the carbyne moiety at the monomeric iron center, typically achieved through the incorporation of heteroatoms in the Fe≡CXR form (where X = O or NR')[12–16]. This stabilization often involves the removal of an –OR group from the carbene group of the Fe=C(OR)R' complex or through electrophilic addition to a cyanide ligand. Notably, Peters reported high valent $Fe^{IV} \equiv CCH_3$ and $[Fe^{V} \equiv CCH_3]^+$ complexes (**I**, Fig. 1a) resulting from an uncommon sequential reductive protonation process of an iron-acetylene compound[17].

In addition to monomeric iron carbyne complexes, Casey and co-workers have synthesized the bridging-methylidyne diiron complex **II** by performing hydride abstraction from the methylene precursor[18–20]. Marchetti and co-workers have developed a convenient two-step synthetic route using $[Cp_2Fe_2(CO)_4]$ to access diiron bridging aminocarbyne compounds **III**[21–23]. These complexes have demonstrated intriguing structural and reactivity features, including reactions with alkenes and diazo compounds, as well as the insertion of alkynes into the iron-carbon bonds. In the pursuit of modeling the structure and functionalities of nitrogenases[24–27], recent advancements in iron carbyne chemistry have led to the synthesis of iron-based heteronuclear cubic clusters (**IV**)[28] and the open-shell diiron hydride complex (**V**)[29], featuring bridging carbyne ligands by the group of Agapie.

Bimetallic cooperation strategy is a powerful tool for exploring bond cleavage and formation in inorganic and organometallic chemistry[30]. Given the crucial role of molybdenum in modulating the electronic properties of the iron–molybdenum cofactor (FeMoco)[31,32], bioinspired Fe-Mo complexes are highly promising for the activation of small molecules[31–33]. Particularly, FeMoco effectively facilitate the reduction of various carbon-based unsaturated substrates such as acetylene (C_2H_2) and carbon monoxide, utilizing protons and electrons (H^+/e^-)[34,35]. Investigating the binding and activation of C_2H_2 with bimetallic Fe-Mo complex could yield a variety of intriguing metal-carbon intermediates such as vinyl and carbyne complexes, offering valuable insights into the interactions and transformations of unsaturated hydrocarbons with abundant metals[17,36–40].

[1]College of Chemistry, Beijing Normal University, 100875 Beijing, China. [2]School of Chemistry and Chemical Engineering, Shandong University, 250100 Jinan, China. [3]Davenport Chemical Research Laboratories, Department of Chemistry, University of Toronto, 80 St. George Street, Toronto, ON M5S 3H6, Canada. ✉e-mail: d.song@utoronto.ca; wwg@bnu.edu.cn

https://doi.org/10.1038/s41467-024-52116-9

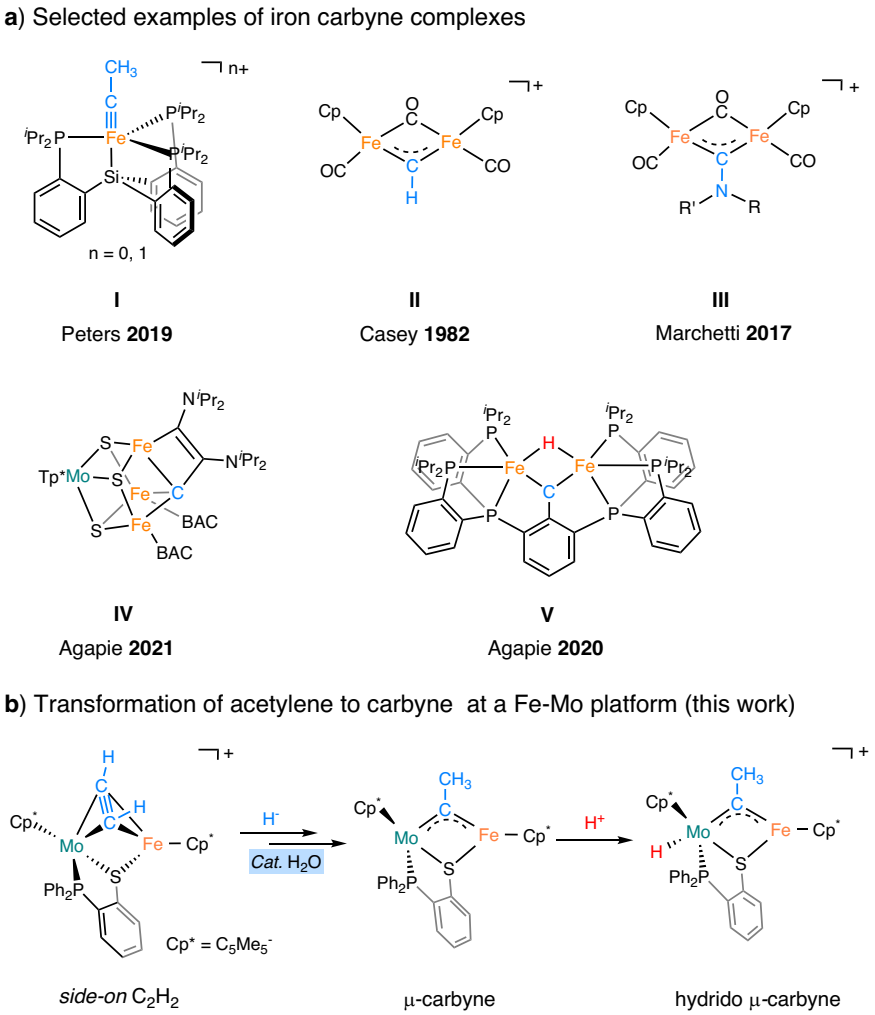

Fig. 1 | Examples of iron-based carbyne complexes. a Selected examples of iron carbyne complexes. **b** Transformation of acetylene to carbyne at a Fe-Mo platform.

Our previous studies demonstrated that molybdenum-acetylene complex Cp*Mo(η^2-C_2H_2)(1,2-$PPh_2C_6H_4S$) transforms to a cationic vinylthioether complex upon protonation[41], while activation of C_2H_2 by Cp*Fe(1,2-$Cy_2PC_6H_4S$) results in the formation of ethenylidene and carbene moieties[40]. In this study, we introduce a bimetallic strategy for the conversion of C_2H_2 into carbyne (Fig. 1b). By integrating Cp*Fe and Cp*Mo moieties within an unsymmetrical phosphino-thiolate coordination sphere, the cationic FeMo complex, [**1**-C_2H_2]BAr_4^F, binds C_2H_2 crosswise the Fe···Mo vector in a double side-on fashion. This coordination mode allows for the transformation of C_2H_2 to a μ-η^1:η^2-CH = CH_2 unsaturated hydrocarbon fragment, which undergoes H-migration catalyzed by H_2O to form a μ-carbyne moiety. Further investigations revealed that protonation of either the vinyl or the neutral carbyne compound affords a hydrido carbyne complex.

Results

Bridging acetylene complex

Upon treating a THF solution of Cp*Mo(η^2-C_2H_2)(1,2-$PPh_2C_6H_4S$)[41] (Mo-C_2H_2) with 0.5 equivalent of [Cp*Fe(μ-Cl)]$_2$ and one equivalent of $NaBAr_4^F$ at −30 °C, a distinct color change from olive green to deep blue occurred (Fig. 2). The resulting product, [**1**-C_2H_2]BAr_4^F, was isolated in an 88% yield and thoroughly characterized by NMR, Raman spectroscopy, and single crystal X-ray diffraction. The ^{31}P NMR spectrum of [**1**-C_2H_2]BAr_4^F exhibits a singlet signal at δ 79.5, upfield shifted compared to δ 97.5 observed for the parent molybdenum-acetylene adduct. In contrast to the broad ^{1}H resonances at δ 9.48 and 10.49 for the η^2-C_2H_2 ligand in the Mo-C_2H_2 complex, the two acetylic protons in [**1**-C_2H_2]$^+$ display two sharp peaks at δ 9.55 (d, $^3J_{P\text{-}H}$ = 13.2 Hz) and 10.48 (s). According to the ^{1}H–^{13}C HSQC studies (Supplementary Fig. 9), the acetylene ^{13}C signals also shifted upfield to δ 162.0 and 160.2 in comparison to Mo-C_2H_2 (δ 190.3 and 184.9). In the Raman spectrum, [**1**-C_2H_2]$^+$ exhibits a sharp $\nu_{C\equiv C}$ band at 1470 cm^{-1}, representing a significant red shift compared to free C_2H_2 (1974 cm^{-1})[42–44] and the Mo-C_2H_2 complex (1507 cm^{-1}, Supplementary Fig. 1). These findings imply a substantial weakening of the C ≡ C triple bond in [**1**-C_2H_2]$^+$, suggesting that the heteronuclear constituent plays a more significant role in C≡C bond activation.

Crystallographic analysis of [**1**-C_2H_2]$^+$ revealed that the Cp*Mo(1,2-$Ph_2PC_6H_4S$) and Cp*Fe$^+$ fragments are linked by the sulfur of the phosphino–thiolate ligand (Fig. 3). A C_2H_2 molecule bound crosswise the Fe–Mo vector through a μ-η^2:η^2-coordination fashion with torsion angle of ~85° between the C–C and Fe–Mo vectors. The Fe–Mo distance of 2.4718(6) Å falls within the sum of covalent radii of Fe (low spin, 1.32 Å) and Mo (1.54 Å)[45]. In comparison to free C_2H_2 ($d_{C\equiv C}$ = 1.181(7) Å)[44], the C ≡ C bond length in [**1**-C_2H_2]$^+$ is elongated to 1.326(6) Å, similar to that of C_2H_4 ($d_{C=C}$ = 1.337(3) Å)[46,47]. This C–C bond is much longer than that in (Cp*Fe)$_2$(1,2-SC_6H_4S)(μ-C_2H_2) (1.181(7) Å)[39]. These structural parameters indicate that the C ≡ C triple bond is significantly weakened due to the strong π back-donation from the heterometallic centers to the π* orbitals. The Mo–C lengths are nearly identical, averaging ~2.10 Å. In contrast, the two Fe–C bond lengths differ much, measuring 1.969(4) Å for Fe–C1 and 2.124(4) Å for Fe–C2.

https://doi.org/10.1038/s41467-024-52116-9

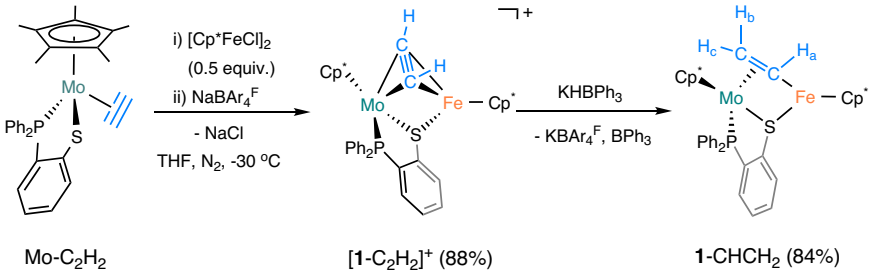

Fig. 2 | Synthesis and reduction of the C_2H_2-bridged Fe–Mo complex.

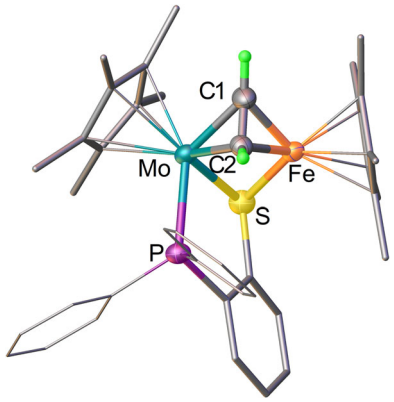

Fig. 3 | Crystal structure of $[\mathbf{1}\text{-}C_2H_2]^+$ with 50% probability thermal ellipsoids. For clarity, the counterion $[BAr_4^F]^-$ and hydrogen atoms except the acetylic protons are omitted, and the phenyl groups and Cp* rings are drawn as lines. Selected bond distances (Å) and angles (deg): Mo-P 2.4836(9), Mo–S 2.3281(9), Mo–C1 2.097(4), Mo–C2 2.110(4), C1–C2 1.326(6), Fe–S 2.2448(11), Fe–C1 1.969(4), Fe–C2 2.124(4), Fe–Mo 2.4718(6); Fe–S–Mo, 65.41(3).

The longer C2–Fe bond and the less hindered C2 are likely responsible for the regio-selectivity in the reaction of $[\mathbf{1}\text{-}C_2H_2]^+$ with hydride (vide infra).

FeMo vinyl complex

The activation of C_2H_2 at the cationic FeMo platform enables it to undergo hydride addition. Treatment of $[\mathbf{1}\text{-}C_2H_2]^+$ with one equivalent of $KHBPh_3$ ($\Delta G_H^- = 36$ kcal·mol^{-1})[48] in THF gradually changes the solution color from deep blue to dark green (Fig. 2). The new ^{31}P NMR signal at 104.6 ppm indicates the formation of a new species in the reaction mixture, from which the vinyl-bridged Fe–Mo complex (**1**-$CHCH_2$) can be isolated in an 84% yield. In the ^{1}H NMR spectrum, distinct resonances can be observed at δ 12.12 (H_a, apparent t, $J_{H\text{-}H} = 8.0$ Hz), 1.86 (H_b, apparent d, J_{ab} (*cis*) = 7.8 Hz), and δ 2.57 (H_c, apparent dd, J_{ac}(*trans*) = 8.9 Hz, $^3J_{P\text{-}Hc} = 15.1$ Hz), which are assigned to the μ-$CHCH_2$ group based on ^{1}H–^{1}H COSY studies (Supplementary Fig. 13). Additionally, the ^{1}H–^{13}C HSQC spectrum confirms the presence of the vinyl ligand, displaying ^{13}C signals at δ 199.0 and 46.4 for the μ-CH and -CH_2 units, respectively (Supplementary Fig. 14). In contrast, the mononuclear Mo-C_2H_2 complex is unreactive toward both $KHBPh_3$ and $LiHBEt_3$, highlighting the reactivity of the cationic FeMo acetylene complex.

In the solid-state structure of **1**-$CHCH_2$, the Mo and Fe centers are unsymmetrically bridged by a μ-η^1,η^2-CH = CH_2 ligand (Fig. 4a). The Mo, C1, Fe, and S atoms are coplanar, as indicated by the sum of interior angles (~360°). Furthermore, the vinyl group is π-bonded to the Mo center, with Mo–C distances of 2.107(4) and 2.301(5) Å, comparable to those in other Mo-η^2-alkene compounds[49–51]. Upon reduction, the C1–C2 bond lengthens to 1.404(7) Å, resembling a typical C = C double bond[47]. Compared to 2.4718(6) Å in $[\mathbf{1}\text{-}C_2H_2]^+$, the Fe–Mo distance is elongated by 0.06 Å, measuring 2.5313(8) Å in **1**-$CHCH_2$, due to the change of the bridging C_2H_2 ligand from a doubly π-bound alkyne to a σ, π-vinyl.

H_2O-promoted carbyne formation

Early studies by Casey demonstrated that the rearrangement of cationic μ-alkylidyne complexes $[Cp_2(CO)Fe_2(\mu\text{-}CO)(\mu\text{-}CCH_2R)]^+$ to the μ-alkenyl complexes $[Cp_2(CO)Fe_2(\mu\text{-}CO)(\mu\text{-}CHCHR)]^+$ occurs at elevated temperature, and the alkyl substituent (R) on the β-carbon accelerates the reaction[19]. Conversely, we discovered that in the presence of catalytic amounts of water, **1**-$CHCH_2$ rearranges to a carbyne compound **1**-CCH_3 through the migration of the proton from the Fe–C*H* unit to the -CH_2 group (Fig. 5). The reaction was conducted in a C_6D_6 solution containing 30 ppm of H_2O at room temperature (see Supplementary Information, Kinetic Studies). As monitored by ^{1}H NMR spectra, the characteristic vinyl proton resonances at δ 12.12 (1H), δ 2.57 (1H), and δ 1.86 (1H) gradually disappear, while a singlet signal for the μ-C*CH*$_3$ group at δ 4.46 emerges. After 6 h, the ^{31}P NMR spectrum only shows a new signal at δ 93.3, indicating the complete conversion of **1**-$CHCH_2$ (^{31}P NMR, δ 104.6) to **1**-CCH_3. The ^{1}H–^{13}C HSQC and HMBC studies confirmed the formation of the carbyne moiety with ^{13}C chemical shifts at δ 378.6 ($^2J_{P\text{-}C} = 8.9$ Hz, μ-*C*CH_3) and δ 41.5 (μ-C*C*H_3), respectively. In contrast, the tautomerization of the vinyl group was not observed in dried solvents such as benzene, toluene, or THF.

The role of water in the conversion of **1**-$CHCH_2$ to **1**-CCH_3 was further probed through a deuterium labeling experiment by adding 1 equivalent of D_2O to the C_6H_6 solution. After reaction at room temperature for 30 min, ^{2}H and ^{1}H NMR studies indicated the deuterium atom was unequivocally incorporated into the methyl group of the carbyne ligand (Fig. 5, Supplementary Figs. 26 and 27). This outcome suggests that water serves as a proton relay and participates in the proton migration process[52,53]. Notably, other protonic reagents such as MeOH, also catalyzed the proton transfer from the vinyl group to a bridging carbyne (see Supplementary Figs. 42 and 43).

Kinetic studies on the isomerization process were conducted with a catalytic amount (30 ppm) of water using ^{1}H NMR spectroscopy (Supplementary Fig. 32). Logarithmic plots reveal first-order kinetics for **1**-$CHCH_2$ → **1**-CCH_3, with a rate constant (k) of 4.09×10^{-3} min^{-1} at 298 K. Further investigations showed that the temperature significantly affects the rearrangement rate. Independent rate measurements at 45 °C yielded $k = 11.0 \times 10^{-3}$ min^{-1}, approximately 30 times faster than the rate at −5 °C (3.7×10^{-4} min^{-1}). An Eyring plot of ln(k/T) versus T^{-1} provided the activation parameters: $\Delta H^{\ddagger} = 10.8$ kcal mol^{-1} and $\Delta S^{\ddagger} = -41.5$ cal·mol^{-1} K^{-1}. These values yield a $\Delta G^{\ddagger}$ value of 23.2 kcal mol^{-1} at 298 K (Fig. 4c). We also found that the water concentration has a significant effect on the rate of the tautomerization, and the reaction order in water was determined to be 0.52 at room temperature (Supplementary Fig. 40 and Table 2), suggesting a possible involvement of water in a pre-equilibrium before the turnover-determining step.

The molecular structure of **1**-CCH_3 was confirmed by X-ray crystallographic analysis (Fig. 4b). In comparison to **1**-$CHCH_2$, the Mo and Fe centers in **1**-CCH_3 are bridged by a methyl-substituted carbyne,

https://doi.org/10.1038/s41467-024-52116-9

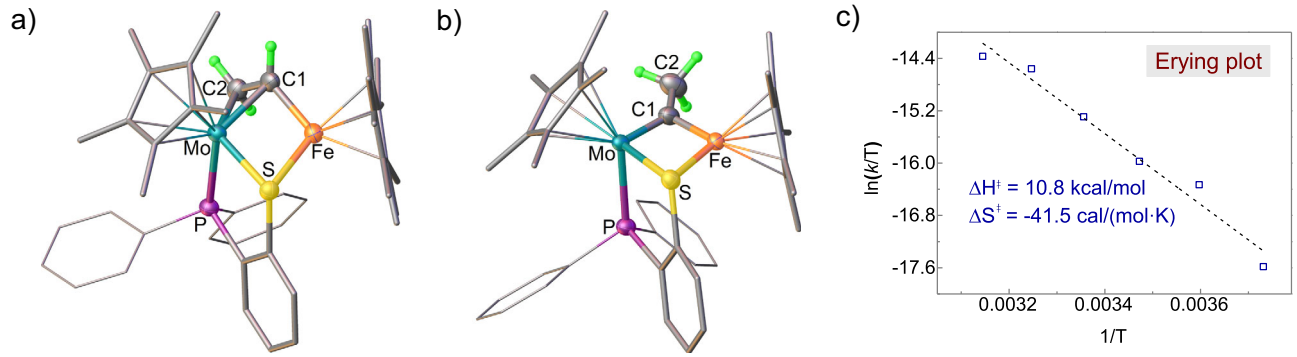

Fig. 4 | Structural characterization and kinetic studies. Solid-state structures of **a** **1**-$CHCH_2$ and **b** **1**-CCH_3 with 50% probability thermal ellipsoids. For clarity, only the hydrogen atoms at vinyl and carbyne ligands are shown, and the phenyl groups are drawn as lines. Selected bond distances (Å) and angles (deg): for **1**-$CHCH_2$, Fe–Mo 2.5313(8), Mo–P 2.4541(11), Mo–S 2.3397(11), Mo–C1 2.107(4), Mo–C2 2.301(5), C1–C2 1.404(7), Fe–S 2.2193(13), Fe–C1 1.962(5), Fe–S–Mo, 67.39(4), Fe–C1–Mo, 76.85(16); for **1**-CCH_3, Fe–Mo 2.5167(5), Mo–P 2.4032(8), Mo–S 2.3424(8), Mo–C1 1.905(3), C1–C2 1.470(5), Fe–S 2.2512(8), Fe–C1 1.901(3), Fe–S–Mo, 66.41(2), Fe–C1–Mo, 82.79(13). **c** Eyring plot of the conversion **1**-$CHCH_2$ → **1**-CCH_3 in d_8-toluene with 30 ppm of H_2O.

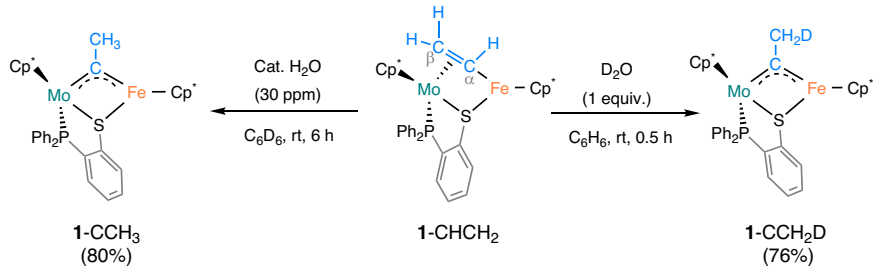

Fig. 5 | Water-catalyzed rearrangement of **1**-$CHCH_2$ to **1**-CCH_3.

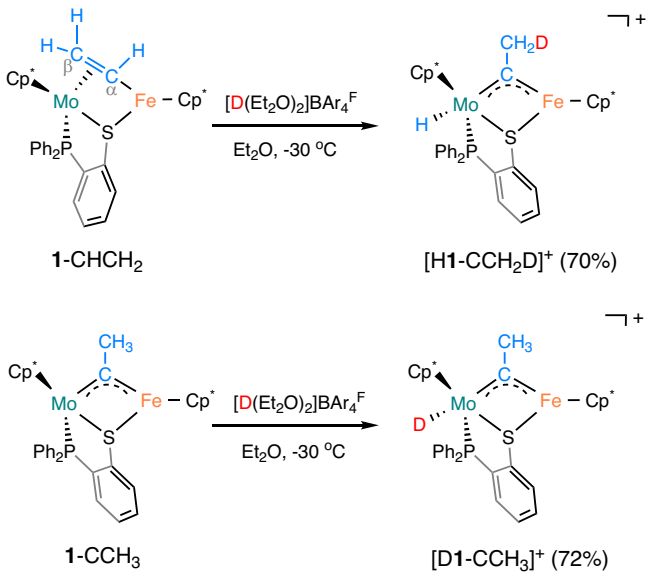

Fig. 6 | Protonation of **1**-$CHCH_2$ and **1**-CCH_3 with $D(Et_2O)_2BAr_4^F$.

rather than the σ, π-vinyl moiety. The Mo–Fe distance of 2.5167(5) Å is slightly shorter than that in **1**-$CHCH_2$ (2.5313(8) Å). The Mo–C1 and Fe–C1 bond lengths are 1.905(3) and 1.901(3) Å, respectively, which are comparable to those observed in [$CpMoFe(\mu\text{-}CAr)(CO)_5$] (Ar = 2,6-$C_6H_3Me_2$)[54]. Given that the covalent radius of Mo is much larger compared to Fe, the nearly identical Mo–C and Fe–C bond lengths suggest that the carbon-metal π bond is predominantly situated on the Mo side. Furthermore, the C1–C2 bond length of 1.470(5) Å is intermediate between the typical C–C single bonds (1.54 Å)[55] and C = C double bonds (1.339(1) Å)[47], and is closer to that of a C–C single bond. It is worth noting that classic alkylidyne ligands lacking hetero-substituents are scarce[16,17].

Hydrido carbyne complex

Surprisingly, both the vinyl complex and the carbyne complex can be protonated to afford a hydrido carbyne complex, [H**1**-CCH_3]$^+$. When an Et_2O solution of **1**-$CHCH_2$ or **1**-CCH_3 was treated with $H(Et_2O)_2BAr_4^F$ at −30 °C, ^{31}P NMR studies indicated that the two reactions gave the same product, displaying a common signal at δ 81.8. The ^1H NMR spectrum showed a characteristic hydride signal at δ − 2.78 (doublet, $^2J_{P\text{-}H}$ = 75 Hz), indicating the formation of a Mo–H species. The μ-CCH_3 proton signal was observed at δ 5.09 (s), and the bridging carbon μ-CCH_3 displayed a ^{13}C resonance at δ 404.5. HRMS studies confirmed the formation of [H**1**-CCH_3]$^+$ with m/z = 745.1613 (Cald. 745.1618).

Deuterium labeling experiments were also performed to gain deeper insights into the protonation reactions (Fig. 6). Upon treatment with $D(Et_2O)_2BAr_4^F$, **1**-$CHCH_2$ yielded [H**1**-CCH_2D]$^+$ as evidenced by ^1H and ^2H NMR studies (Supplementary Figs. 26 and 27). This suggests that protonation occurs at the β-vinyl carbon, followed by oxidative addition of the α-C–H onto molybdenum. In contrast, the reaction of **1**-CCH_3 with $D(Et_2O)_2BAr_4^F$ led to protonation occurring at the molybdenum center, giving rise to a deuteride species [D**1**-CCH_3]$^+$ (Supplementary Figs. 28–30).

The crystallographic analysis of [H**1**-CCH_3][BAr_4^F] consistently revealed disordered structures. However, when replacing the counter anion from [BAr_4^F]$^-$ to [$B(C_6F_5)_4$]$^-$, we were able to obtain X-ray-quality single crystals. The solid-sate structure of [H**1**-CCH_3]$^+$ exhibits a similar skeleton to the neutral μ-carbyne compound (Fig. 7). The bond lengths of C1–C2 (1.461(8) Å) and Fe–C1 (1.845(6) Å) are close to those observed in **1**-CCH_3. However, the Mo–C1 bond shows noticeable

elongation, i.e. 1.959(6) Å for [H**1**-CCH_3]$^+$ *vs.* 1.905(3) Å for **1**-CCH_3. The hydride position was refined, revealing a Mo–H bond length of 1.67(6) Å, consistent with the previously reported Mo(VI)–H species[56,57]. Note that [H**1**-CCH_3]$^+$ represents the first heteronuclear hydrido μ-carbyne complex. Spectroscopic studies have shown that the active states of FeMoco feature hydride ligands[58–60], and metal-hydride intermediates have been proposed to be involved in the reduction of acetylene by nitrogenase[34,61,62]. Therefore, [H**1**-CCH_3]$^+$ can serve as a promising synthetic entry point for the development of FeMoco models.

Mechanism studies

To elucidate the mechanism of water-promoted proton transfer process, DFT studies were performed (Fig. 8). According to the calculations, the reaction is proposed to start with the coordination of H_2O onto the iron center of **1**-$CHCH_2$, leading to the formation of **Int1** (3.5 kcal mol^{-1}). This coordination enhances the acidity of H_2O, facilitating the turnover-determining proton transfer to the CH_2 group to give **Int2** (7.1 kcal mol^{-1}) via **TS1** (24.4 kcal mol^{-1}). We also measured the kinetic isotope effect (KIE) by comparing the initial reaction rates in the presence of H_2O and D_2O (29.2 mol%) in independent runs at 298 K. The normal primary KIE value ($k_H/k_D = 3.70$) is consistent with a turnover-determining protonation step. **Int2** features a bridging alkylidene between the Mo and Fe centers and β–agostic interaction between the CH_3 group and the Mo center. The subsequent reorientation of the bridging alkylidene gives **Int3** (7.2 kcal mol^{-1}) via **TS2** (18.1 kcal mol^{-1}). Such an isomerization brings the α-proton of the bridging alkylidene and the iron-bound OH to the *syn* configuration with respect to the C–Fe bond for the facile proton transfer via **TS3** (11.4 kcal·mol^{-1}) to afford **Int4** (−1.8 kcal mol^{-1}). The dissociation of H_2O from the iron center of **Int4** gives the final product **1**-CCH_3 (−9.6 kcal mol^{-1}). The well-ordered rate-determining transition state **TS1** can also account for the negative experimental $\Delta S^{\ddagger}$. The computed energetic span of 24.4 kcal mol^{-1} is similar to the experimental result (23.2 kcal mol^{-1}). In contrast, a few alternative routes involving water were ruled out for thermodynamic reasons (See Supplementary Information, DFT Calculations). The computed direct isomerization of **1**-$CHCH_2$ to **1**-CCH_3 has a free energy barrier of 38.6 kcal mol^{-1}, which is consistent with the lack of reactivity in thoroughly dried solvents at ambient temperature and the barrier (>31.0 kcal mol^{-1}) estimated by Casey[19].

In summary, we have demonstrated the transformation of C_2H_2 into a bridging carbyne ligand on a bioinspired FeMo platform. The incorporation of Cp*Fe and Cp*Mo moieties into an unsymmetrical phosphino-thiolate coordination environment enables the activation of C_2H_2 crosswise the Fe–Mo vector and its subsequent reduction by a hydride, resulting in the formation of a vinyl group (μ-η^1,η^2-$CH=CH_2$). Mechanism studies reveal that water plays a significant role as a proton shuttle in the tautomerization reaction, converting the vinyl group into a carbyne. This water-promoted C–H bond cleavage and formation are reminiscent of biological C–H bond activation processes observed in the enzymes such as cytochrome P450[63,64]. Intriguingly, both the vinyl and the carbyne complexes undergo protonation, leading to the same hydrido carbyne complex. Deuterium labeling experiments reveal that the vinyl protonation occurs at the β-carbon, whereas the molybdenum site in the carbyne complex is more prone to protonation compared to the bridging carbyne carbon (Mo-*C*(CH_3)-Fe). In general, this MoFe system offers a synthetic method for the incorporation of a bridging carbon and hydride ligands into an Fe-S-Mo framework starting from common, simple organic substrates.

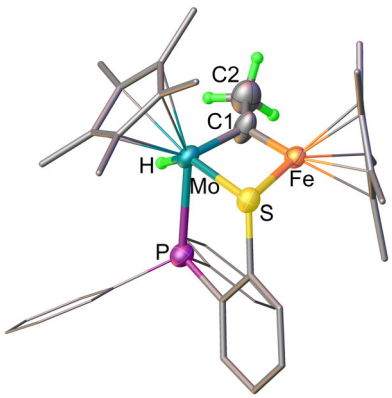

Fig. 7 | Solid-state structure of [H1-CCH_3]$^+$ with 50% probability thermal ellipsoids. For clarity, the counterion [$B(C_6F_5)_4$]$^-$ and most hydrogen atoms are omitted, and the two phenyl groups at the phosphorus site are drawn as lines. Selected bond distances (Å) and angles (deg): Mo–H 1.67(6), Mo–P 2.4672(14), Mo–S 2.3803(14), Mo–C1 1.959(6), C1–C2 1.461(8), Fe–S 2.2212(14), Fe–C1 1.845(6), Mo–Fe 2.5469(8); Fe–S–Mo, 67.11(4); Fe–C1–Mo, 84.0(2).

Methods

General procedures for kinetic studies on the conversion of 1-$CHCH_2$ to 1-CCH_3

The solvent d_8-toluene was dried over 3 Å molecular sieves for 3 days (residual water content 0.9 ± 0.3 ppm)[65]. A d_8-toluene solution (contain 30 ppm H_2O) was then prepared by adding 3 μL H_2O to 100 mL predried d_8-toluene. A 26.9 mM solution of **1**-$CHCH_2$ was prepared by dissolving **1**-$CHCH_2$ (10.0 mg, 0.013 mmol) in 500 μL d_8-toluene (contain 30 ppm H_2O, 4.38 mol% with respect to **1**-$CHCH_2$). The solution was transferred to a J. Young NMR tube and placed into a

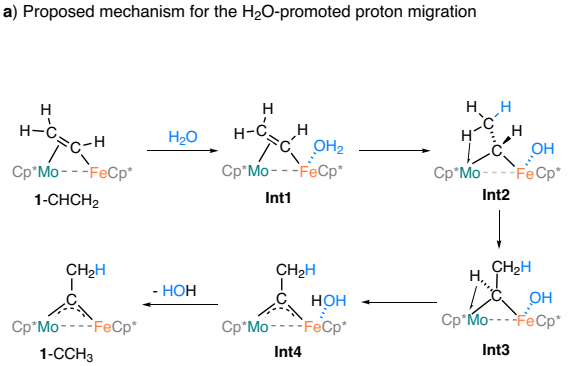

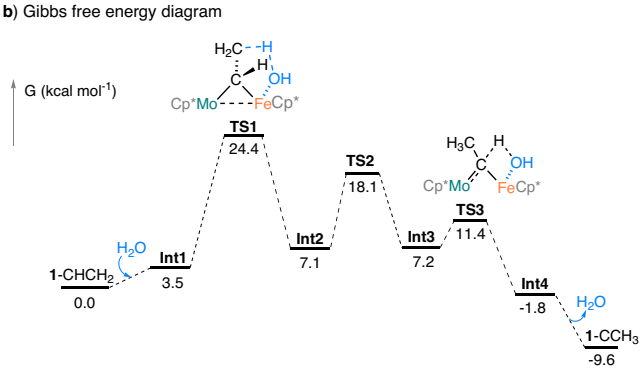

Fig. 8 | DFT studies. a Proposed mechanism for water-catalyzed isomerization of **1**-$CHCH_2$. **b** Computed Gibbs free energy profile (in kcal mol^{-1}, at 298 K, 1 mol L^{-1} concentration). All structures were optimized in full (M11L, def2tzvp, PCM). For clarity, the drawings of all MoFe complexes were simplified by omitting the *P*,*S*-ligand. For computational details, see the DFT Calculations in Supplementary Information.

temperature-calibrated NMR probe (−5 to 45 °C). ^{1}H NMR spectra were collected until ~30% conversion to **1**-CCH_3 completed. No side products were evidenced by ^{1}H NMR spectroscopy. The concentrations of **1**-$CHCH_2$ and **1**-CCH_3 were determined by the integration of the vinyl signal −C*H*CH_2 at δ 12.03 and the methyl signal μ−CC*H*$_3$ at δ 4.42, respectively ($SiEt_4$ as internal standard). The resulting data was fit to a first-order kinetics plot. The rate constants at −5, 5, 15, 25, 35, and 45 °C were determined from the time dependence plots of ln[**1**-$CHCH_2$].

Data availability

Crystallographic data for the structures reported in this article have been deposited at the Cambridge Crystallographic Data Centre, under deposition numbers CCDC 2321830 ([**1**-C_2H_2]BAr_4^F), 2321832 (**1**-$CHCH_2$), 2321833 (**1**-CCH_3), 2321834 ([H**1**-CCH_3][$B(C_6F_5)$]. All other data related to experimental procedures, spectroscopic characterizations, kinetic studies, computational details and crystallographic data are included in Supplementary Information. Atomic coordinates of optimized structures are included in a.xyz file named Source Data. All data are available from the corresponding author upon request. Source data are provided with this paper.

References

1. Fischer, E. O. et al. Trans-Halogeno[alkyl(aryl)carbyne]tetracarbonyl complexes of chromium, molybdenum, and tungsten-A new class of compounds having a transition metal-carbon triple bond. *Angew. Chem. Int. Ed.* **12**, 564–565 (1973).
2. McLain, S. J. et al. Multiple metal-carbon bonds. 10. Thermally stable tantalum alkylidyne complexes and the crystal structure of Ta(η^5-C_5Me_5)(CPh)(PMe_3)$_2$Cl. *J. Am. Chem. Soc.* **100**, 5962–5964 (1978).
3. Wei, R. et al. Synthesis and reactivity of copper carbyne anion complexes. *Nat. Synth.* **2**, 357–363 (2023).
4. Chen, S. et al. Addition of alkynes and osmium carbynes towards functionalized d_π–p_π conjugated systems. *Nat. Commun.* **11**, 4651 (2020).
5. Cui, M. & Jia, G. Organometallic chemistry of transition metal alkylidyne complexes centered at metathesis reactions. *J. Am. Chem. Soc.* **144**, 12546–12566 (2022).
6. Fürstner, A. Alkyne metathesis on the rise. *Angew. Chem. Int. Ed.* **52**, 2794–2819 (2013).
7. Yiannakas, E., Grimes, M. I., Whitelegge, J. T., Fürstner, A. & Hulme, A. N. An alkyne-metathesis-based approach to the synthesis of the anti-malarial macrodiolide samroiyotmycin A. *Angew. Chem. Int. Ed.* **60**, 18504–18508 (2021).
8. Bellone, D. E., Bours, J., Menke, E. H. & Fischer, F. R. Highly selective molybdenum ONO pincer complex initiates the living ring-opening metathesis polymerization of strained alkynes with exceptionally low polydispersity indices. *J. Am. Chem. Soc.* **137**, 850–856 (2015).
9. von Kugelgen, S., Bellone, D. E., Cloke, R. R., Perkins, W. S. & Fischer, F. R. Initiator Control of Conjugated Polymer Topology in Ring-Opening Alkyne Metathesis Polymerization. *J. Am. Chem. Soc.* **138**, 6234–6239 (2016).
10. Münster, K. & Walter, M. D. *Comprehensive Organometallic Chemistry IV*. 7, 46–184 (Elsevier, 2022).
11. Marchetti, F., *Comprehensive Organometallic Chemistry IV*. 7, 210–257 (Elsevier, 2022).
12. Fischer, E. O., Schneider, J. & Neugebauer, D. [$(CO)_3PPh_3FeCN^iPr_2]^+$, a novel stable carbyneiron complex cation. *Angew. Chem.* **23**, 820–821 (1984).
13. Mokhtarzadeh, C. C., Moore, C. E., Rheingold, A. L. & Figueroa, J. S. Terminal iron carbyne complexes derived from arrested CO_2 reductive disproportionation. *Angew. Chem. Int. Ed.* **56**, 10894–10899 (2017).
14. Rittle, J. & Peters, J. C. Proton-coupled reduction of an iron cyanide complex to methane and ammonia. *Angew. Chem. Int. Ed.* **55**, 12262–12265 (2016).
15. Lee, Y. & Peters, J. C. Silylation of iron-bound carbon monoxide affords a terminal Fe carbyne. *J. Am. Chem. Soc.* **133**, 4438–4446 (2011).
16. Rao, J. et al. Triplet iron carbyne complex. *J. Am. Chem. Soc.* **145**, 25766–25775 (2023).
17. Citek, C., Oyala, P. H. & Peters, J. C. Mononuclear Fe(I) and Fe(II) acetylene adducts and their reductive protonation to terminal Fe(IV) and Fe(V) carbynes. *J. Am. Chem. Soc.* **141**, 15211–15221 (2019).
18. Casey, C. P., Fagan, P. J. & Miles, W. H. Synthesis and interconversions of dinuclear iron complexes with μ-methyl, μ-methylene, and μ-methylidyne ligands. *J. Am. Chem. Soc.* **104**, 1134–1136 (1982).
19. Casey, C. P., Marder, S. R. & Adams, B. R. Interconversion of μ-alkylidyne and μ-alkenyl diiron Complexes. *J. Am. Chem. Soc.* **107**, 7700–7705 (1985).
20. Casey, C. P. et al. Hydrocarbation-formation of diiron μ-alkylidyne complexes from the addition of the carbon-hydrogen bond of a μ-methylidyne complex across alkenes. *J. Am. Chem. Soc.* **108**, 4043–4053 (1986).
21. Agonigi, G. et al. Regioselective nucleophilic additions to diiron carbonyl complexes containing a bridging aminocarbyne ligand: A synthetic, crystallographic and DFT study. *Eur. J. Inorg. Chem.* **2018**, 960–971 (2017).
22. Marchetti, F. Constructing organometallic architectures from aminoalkylidyne diiron complexes. *Eur. J. Inorg. Chem.* **2018**, 3987–4003 (2018).
23. Biancalana, L. & Marchetti, F. Aminocarbyne ligands in organometallic chemistry. *Coord. Chem. Rev.* **449**, 214203–214256 (2021).
24. Lancaster, K. M. et al. X-ray emission spectroscopy evidences a central carbon in the nitrogenase iron-molybdenum cofactor. *Science* **334**, 974–977 (2011).
25. Čorić, I. & Holland, P. L. Insight into the iron-molybdenum cofactor of nitrogenase from synthetic iron complexes with sulfur, carbon, and hydride ligands. *J. Am. Chem. Soc.* **138**, 7200–7211 (2016).
26. Liu, L., Rauchfuss, T. B. & Woods, T. J. Iron carbide–sulfide carbonyl clusters. *Inorg. Chem.* **58**, 8271–8274 (2019).
27. Joseph, C., Cobb, C. R. & Rose, M. J. Single-step sulfur insertions into iron carbide carbonyl clusters: unlocking the synthetic door to FeMoco analogues. *Angew. Chem. Int. Ed.* **60**, 3433–3437 (2021).
28. Le, L. N. V., Bailey, G. A., Scott, A. G. & Agapie, T. Partial synthetic models of FeMoco with sulfide and carbyne ligands: effect of interstitial atom in nitrogenase active site. *Proc. Natl Acad. Sci. USA* **118**, e2109241118 (2021).
29. Arnett, C. H. & Agapie, T. Activation of an open shell, carbyne-bridged diiron complex toward binding of dinitrogen. *J. Am. Chem. Soc.* **142**, 10059–10068 (2020).
30. Campos, J. Bimetallic cooperation across the periodic table. *Nat. Rev. Chem.* **4**, 696–702 (2020).
31. Hoffman, B. M., Lukoyanov, D., Yang, Z. Y., Dean, D. R. & Seefeldt, L. C. Mechanism of nitrogen fixation by nitrogenase: the next stage. *Chem. Rev.* **114**, 4041–4062 (2014).
32. Jasniewski, A. J., Lee, C. C., Ribbe, M. W. & Hu, Y. Reactivity, mechanism, and assembly of the alternative nitrogenases. *Chem. Rev.* **120**, 5107–5157 (2020).
33. Su, L. et al. A bioinspired iron-molybdenum μ-nitrido complex and its reactivity toward ammonia formation. *Angew. Chem. Int. Ed.* **61**, e202203121 (2022).
34. Seefeldt, L. C. et al. Reduction of substrates by nitrogenases. *Chem. Rev.* **120**, 5082–5106 (2020).
35. Wilson, D. W. N. & Holland, P. L. *Comprehensive Organometallic Chemistry IV*. 15, 41–72 (Elsevier, 2022).
36. Santos, P. C. D. et al. Substrate interactions with the nitrogenase active site. *Acc. Chem. Res.* **38**, 208–214 (2005).
37. Lee, H. et al. An organometallic intermediate during alkyne reduction by nitrogenase. *J. Am. Chem. Soc.* **126**, 9563–9569 (2004).

38. Lee, H. I. et al. Electron inventory, kinetic assignment (En), structure, and bonding of nitrogenase turnover intermediates with C_2H_2 and CO. *J. Am. Chem. Soc.* **127**, 15880–15890 (2005).
39. Yang, D. et al. Reactivity toward unsaturated small molecules of thiolate-bridged diiron hydride complexes. *Inorg. Chem.* **57**, 15198–15204 (2018).
40. Zhang, X., Feng, L., Tung, C.-H. & Wang, W. Transformation of acetylene to ethenylidene, carbene, acetylide, vinyl, and olefin groups with Cp*Fe(1,2-$Cy_2PC_6H_4S$). *Inorg. Chem.* **62**, 18599–18606 (2023).
41. Xue, M. et al. Catalytic hydrogenation of olefins by a multifunctional molybdenum-sulfur complex. *Nat. Commun.* **15**, 797 (2024).
42. Iwashita, Y. Force constants in the acetylene molecule in a cobalt-carbonyl complex and in an excited electronic state. *Inorg. Chem.* **9**, 1178–1182 (1970).
43. Noonikara-Poyil, A., Ridlen, S. G., Fernández, I. & Dias, H. V. R. Isolable acetylene complexes of copper and silver. *Chem. Sci.* **13**, 7190–7203 (2022).
44. Fast, H. & Welsh, H. L. High-resolution raman spectra of acetylene, acetylene-d1, and acetylene-d2. *J. Mol. Spectrosc.* **41**, 203–221 (1972).
45. Cordero, B. et al. (2008) Covalent radii revisited. *Dalton Trans*. 2832.
46. Zenkina, O. V., Keske, E. C., Wang, R. & Crudden, C. M. Double single-crystal-to-single-crystal transformation and small-molecule activation in rhodium NHC complexes. *Angew. Chem. Int. Ed.* **50**, 8100–8104 (2011).
47. Hirota, E. et al. Microwave spectra of deuterated ethylenes: dipole moment and rz structure. *J. Mol. Spectrosc.* **89**, 223–231 (1981).
48. Heiden, Z. M. & Lathem, A. P. Establishing the hydride donor abilities of main group hydrides. *Organometallics* **34**, 1818–1827 (2015).
49. Bezdek, M. J. & Chirik, P. J. Proton-coupled electron transfer to a molybdenum ethylene complex yields a β-Agostic ethyl: structure, dynamics and mechanism. *J. Am. Chem. Soc.* **140**, 13817–13826 (2018).
50. Carmona, E., Marin, J. M., Poveda, M. L., Atwood, J. L. & Rogers, R. D. Preparation and properties of dinitrogen trimethylphosphine complexes of molybdenum and tungsten. 4. Synthesis, chemical properties, and X-ray structure of cis-[$Mo(N_2)_2(PMe_3)_4$]. The crystal and molecular structures of *trans*-[$Mo(C_2H_4)_2(PMe_3)_4$] and *trans,-mer*-[$Mo(C_2H_4)_2(CO)(PMe_3)_3$]. *J. Am. Chem. Soc.* **105**, 3014–3022 (1983).
51. Álvarez, M. Á., Galindo, A., Pérez, P. J. & Carmona, E. Molybdenum and tungsten complexes with carbon dioxide and ethylene ligands. *Chem. Sci.* **10**, 8541–8546 (2019).
52. Ben-Ari, E., Leitus, G., Shimon, L. J. W. & Milstein, D. Metal–ligand cooperation in C–H and H_2 activation by an electron-rich PNP Ir(I) system: facile ligand dearomatization–aromatization as key steps. *J. Am. Chem. Soc.* **128**, 15390–15391 (2006).
53. Iron, M. A., Ben-Ari, E., Cohen, R. & Milstein, D. (2009) Metal–ligand cooperation in the trans addition of dihydrogen to a pincer Ir(I) complex: a DFT study. *Dalton Trans*. 9433.
54. Dossett, S. J. et al. Chemistry of polynuclear metal complexes with bridging carbene or carbyne ligands. Part 79. Synthesis and reactions of the alkylidynemetal complexes [M(≡CR)$(CO)_2$(η-C_5H_5)](R = $C_6H_3Me_2$–2,6, M = Cr, Mo, or W; R = C_6H_4Me-2, C_6H_4OMe-2, or $C_6H_4NMe_2$–4, M = Mo); Crystal structure of the compound [MoFe(μ-$CC_6H_3Me_2$–2,6)$(CO)_5$. *J. Chem. Soc., Dalton Trans*. 2453–2465 (1988).
55. Allen, F. H. et al. Tables of bond lengths determined by X-ray and neutron diffraction. Part 1. Bond lengths in organic compounds. *J. Chem. Soc. Perkin Trans.* **2**, S1 (1987).
56. Abugideiri, F., Kelland, M. A. & Poli, R. Molybdenum complex Cp*$MoH_5(PMe_3)$: a classical polyhydride with a pentagonal-bipyramidal structure and a long T1 relaxation time. *Organometallics* **12**, 2388–2389 (1993).
57. Ohki, Y. et al. Dinuclear Mo_2H_8 complex supported by bulky $C_5H_2tBu_3$ ligands. *Chem. Commun.* **56**, 8035–8038 (2020).
58. Igarashi, R. Y. et al. Trapping H-bound to the nitrogenase FeMo-cofactor active site during H_2 evolution: characterization by ENDOR spectroscopy. *J. Am. Chem. Soc.* **127**, 6231–6241 (2005).
59. Lukoyanov, D., Barney, B. M., Dean, D. R., Seefeldt, L. C. & Hoffman, B. M. Connecting nitrogenase intermediates with the kinetic scheme for N_2 reduction by a relaxation protocol and identification of the N_2 binding state. *Proc. Natl Acad. Sci. USA* **104**, 1451–1455 (2007).
60. Lukoyanov, D., Yang, Z. Y., Dean, D. R., Seefeldt, L. C. & Hoffman, B. M. Is Mo involved in hydride binding by the four-electron reduced (E4) intermediate of the nitrogenase MoFe protein? *J. Am. Chem. Soc.* **132**, 2526–2527 (2010).
61. Arnet, N. A. et al. Synthesis, characterization, and nitrogenase-relevant reactions of an iron sulfide complex with a bridging hydride. *J. Am. Chem. Soc.* **137**, 13220–13223 (2015).
62. Hoffman, B. M., Lukoyanov, D., Dean, D. R. & Seefeldt, L. C. Nitrogenase: a draft mechanism. *Acc. Chem. Res.* **46**, 587–595 (2013).
63. De Visser, S. P. & Shaik, S. A Proton-shuttle mechanism mediated by the porphyrin in benzene hydroxylation by cytochrome P450 enzymes. *J. Am. Chem. Soc.* **125**, 7413–7424 (2003).
64. Mondal, D., Snodgrass, H. M., Gomez, C. A. & Lewis, J. C. Non-native site-selective enzyme catalysis. *Chem. Rev.* **123**, 10381–10431 (2023).
65. Williams, D. B. G. & Lawton, M. Drying of organic solvents: quantitative evaluation of the efficiency of several desiccants. *J. Org. Chem.* **75**, 8351–8354 (2010).

Acknowledgements

W.W. thanks the financial support from the National Natural Science Foundation of China (22022102 and 22071010) and the Natural Science Foundation of Shandong Province (ZR2019ZD45). D.S. thanks the Natural Sciences and Engineering Research Council (NSERC) of Canada for funding (RGPIN-2019-06576). This research was enabled in part by support provided by Sharcnet (www.sharcnet.ca) and Digital Research Alliance of Canada (alliancecan.ca).

Author contributions

W.W., D.S., X.Z., and C.-H.T. conceived and designed the project. X.Z. performed the experiments and interpreted the data. D.S. carried out the computational studies. M.X., Q.-T.Z, and Q.-C.Z assisted with Variable Temperature NMR experiments. W.W., D.S., and X.Z. wrote the manuscript. All authors provided comments on the experiments and the manuscript during its preparation.

Competing interests

The authors declare no competing interests.

Additional information

Supplementary information The online version contains supplementary material available at https://doi.org/10.1038/s41467-024-52116-9.

Correspondence and requests for materials should be addressed to Datong Song or Wenguang Wang.

Peer review information *Nature Communications* thanks Haifeng Qi and the other anonymous reviewer(s) for their contribution to the peer review of this work. A peer review file is available.